Technical Note

Landslides (2025) 22:4013–4027
DOI 10.1007/s10346-025-02598-5
Received: 7 March 2025
Accepted: 16 July 2025
Published online: 8 August 2025

Andrej Novak · Marko Vrabec · Andrej Šmuc

Long-term post-event processes and major reactivation of a complex landslide: 2000–2023 evolution of the Ciprnik landslide, Julian Alps, Slovenia

Abstract The Ciprnik complex landslide in the Planica valley (NW Slovenia) happened on 19. 11. 2000 as a translation slip-debris flow-hyperconcentrated flow event. It was triggered by a combination of the local geological structure (highly fractured beds dipping parallel to the surface), lithology (alternation of thin bedded carbonates and fine-grained clastics), and record-breaking monthly rainfall (613.6 mm in the month of the event). Twenty-three years later, on the night from 24. to 25. 10. 2023, large parts of the landslide reactivated during intense short-duration rainfall, which has a relatively common occurrence (104.2 mm in 24 h). We use 2006–2023 time series of photogrammetrically derived digital elevation models generated from aerial photographs and unmanned aerial vehicle surveys, sedimentological analysis, and meteorological data to (1) analyze decade-scale post-event processes on the Ciprnik landslide following the initial sliding event in November 2000 and (2) to study the October 2023 event and compare it to the November 2000 event. We find that after the initial November 2000 event, the area of the Ciprnik landslide remained unstable with an average annual erosion rate of 1000 to 3500 m^3 of sediment. The 2023 event measured 26,000 m^3 and, despite a different triggering rainfall, again occurred as a translation slip-debris flow-hyperconcentrated flow event exhibiting a strong fining down of sediment (from muddy-sandy-gravel to sandy-silt). This study demonstrates the complexity of triggering thresholds in the aftermath of the main mass movement event. Even in the later events, which have the same transport mechanisms as the original event, the triggering precipitation can differ considerably in duration and magnitude.

Keywords Complex landslide · Translational slip · Debris flow · Hyperconcentrated flow · UAV · Granulometry

Introduction

Mass movements are a natural phenomenon which often produce a devastating effect on infrastructure and may also result in human casualties (Haque et al. 2016). Mountain environments are especially prone to their occurrence, and movements are often, but not exclusively, triggered by intense rainfall events. (Jakob & Hungr 2005, 2005; Guzzetti et al. 2007, 2008; Margottini et al. 2013; Hungr et al. 2014; Haque et al. 2016; Rimal et al. 2025). Mass movements in mountain environments present a risk to lower-lying settlements not only by directly impacting the local population but also due to presenting a significant threat to agricultural, touristic, and leisure industries, typical for the European Alpine region. Since future climate scenarios indicate an increase in landslide activity in the Alpine region (Gariano & Guzzetti 2022; Maraun et al. 2022; Jemec Auflič et al. 2023), it is crucial to investigate these events to better understand the triggering forcings and associated syn- and post-event processes.

Mass movements are determined by geological structure, lithology, slope morphology, land cover, and water flow. They are classified according to the transport mechanism and material properties, each producing unique transport and depositional characteristics, and consequentially their effect on the environment and infrastructure is variable (Varnes 1978; Wilford et al. 2004; Hungr 2005; Hungr et al. 2001, 2014; Church & Jakob 2020; Jakob et al. 2022).

In complex landslides, two or more different materials and/or transport mechanisms are employed in the mass movement event. A complex landslide is therefore defined and described by its movement stages (Cruden & Varnes 1996; Hungr et al. 2014), for example, as a rock slide-debris flow event (e.g., Deline et al. 2011). Since each stage of movement in a complex landslide has different transport and depositional characteristics, their impact on the environment can be very different. It is therefore necessary to investigate the aspects of each stage of a complex landslide and assess its environmental impact.

The Ciprnik complex landslide, triggered on the 19. 11. 2000, is a relatively large landslide located in the Planica valley, NW Slovenia (46.46387 N, 13.72883 E; Fig. 1a). The landslide was defined as a complex landslide type characterized as a translation slip-debris flow-hyperconcentrated flow event (Šmuc et al. 2015). Since the landslide is situated in the uninhabited area within the Triglav National Park, no restoration or remediation works were undertaken after the event, and therefore, the complex Ciprnik landslide presents a unique natural laboratory for studying triggering conditions, post-event processes, and reactivations of preexisting landslide surface without anthropogenic influences.

The focus of this study is on analyzing the triggering conditions and transport-depositional characteristics of mass movements in the aftermath of the main mass wasting event in the case of the Ciprnik complex landslide. As demonstrated by various studies (Rossi et al. 2018; Peternel et al. 2022, 2025; Sun et al. 2024; Sestras et al. 2025; Tsunetaka 2025; and references within), multitemporal unmanned aerial vehicle (UAV) surveys based on the UAV photogrammetry technique are widely used and proved to be highly effective in monitoring post-event processes, movement characterization, and landslide mapping. We employ aerial photography from various sources to derive 2006–2023 time series of photogrammetrically produced digital elevation models (DEMs) of the

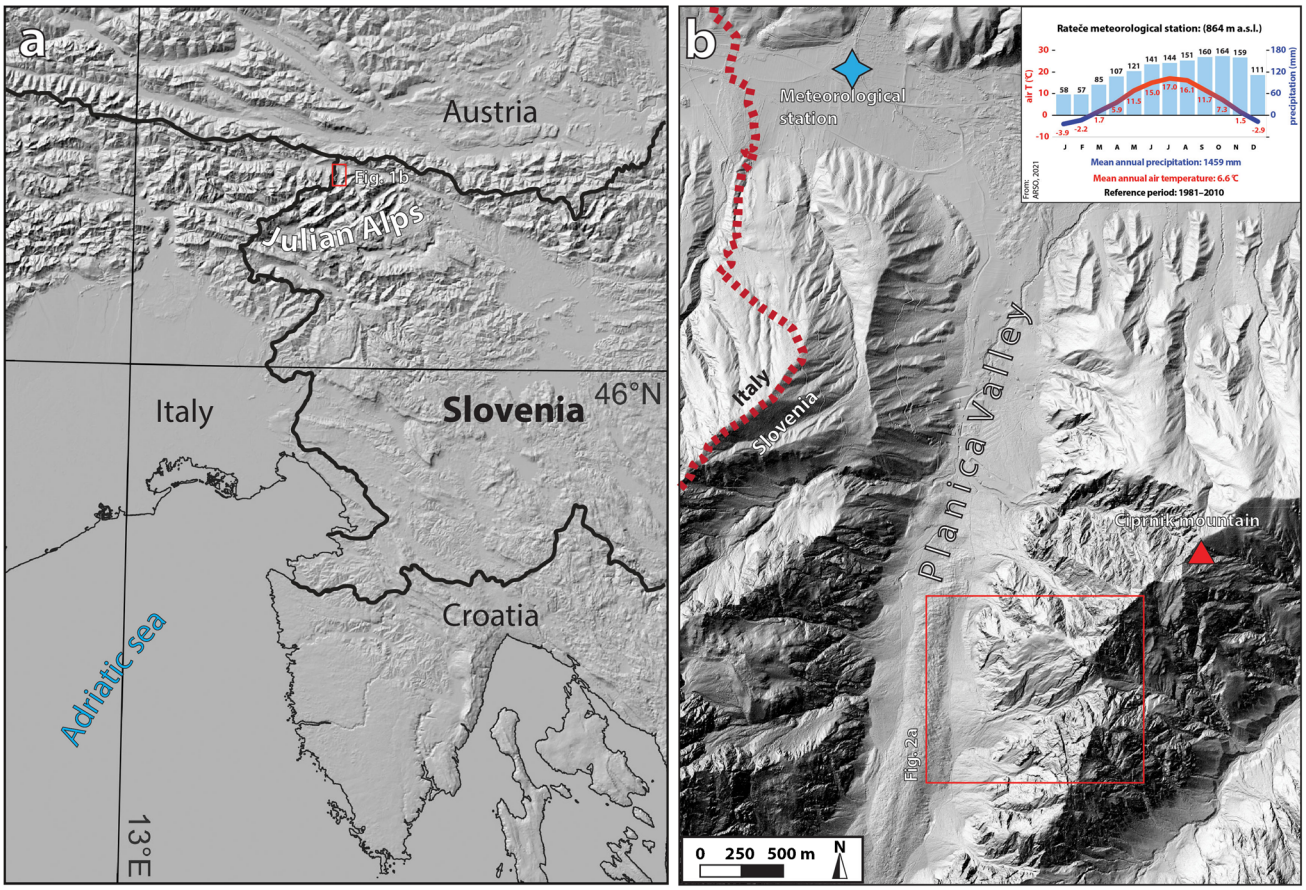

Fig. 1 Characteristics of the research area. **a** Location of the Planica valley in the Julian Alps in NW Slovenia. **b** Location of the Ciprnik complex landslide in the Planica valley and Rateče meteorological station. Climatic conditions of the research area are presented in the climatic diagram

landslide area, to analyze post-2000 event processes and small-scale reactivations and relate them to rainfall triggers.

A major reactivation of the Ciprnik complex landslide happened on the night from 24. to 25. 10. 2023. This event occurred at the same location as the initial event two decades earlier. Both events also share very similar transport and depositional mechanisms, but the triggering rainfall events were markedly different. We present a detailed analysis of the triggering, transport, and depositional mechanisms of the 24. to 25. 10. 2023 event, based on UAV surveys, sedimentological analysis of the transported sediment, and meteorological data. Finally, we compare the November 2000 and October 2023 events.

Geological setting, climatic conditions, and summary of the November 2000 complex landslide movement

The Planica Valley (Fig. 1b) is a typical postglacial U-shaped valley with steep slopes predominately built from Triassic limestones and dolomites (Ogorelec et al. 1984; Celarc 2004; Gale et al. 2015). The stratigraphic succession includes a 50 m thick Tor Formation of Early Upper Triassic age, which is characterized by alternations of claystone, siltstone, marly dolomite, and limestone layers. The Tor Formation outcrops extensively in the southwest slopes of Mt. Ciprnik (Gale et al. 2015).

A permanent meteorological station, collecting daily observations since 1949, is located in the village of Rateče, a few kilometres from the Ciprnik site (ARSO 2023; Fig. 1b). The Planica valley has a climate of alpine environments, with an average annual rainfall of 1453 mm and rainfall maximum occurring in autumn (ARSO 2021a; Fig. 1b).

The year 2000 event was triggered on the night between 18. and 19. 11. 2000, measuring approximately 80,000 m^3 (Komac & Zorn 2007; Zorn & Komac 2008). Before that, the steep slopes of Mt. Ciprnik were predominantly forested with no evidence of pre-existing slope mass movements (Bohinec 1935; Šmuc et al. 2015). At the foot of the mountain, there is an active alluvial fan (Šmuc et al. 2015; Novak et al. 2018). The area of the 2000 event encompasses an altitudinal range from approximately 1010 up to 1500 m a.s.l. (Fig. 2). The complex landslide movement was characterized as a translation slip-debris flow-hyperconcentrated flow event (Šmuc et al. 2015).

Following Šmuc et al. (2015), the Ciprnik complex landslide is divided into four distinct units, which reflect the landslide evolution. The initial movement occurred as translational slip at the altitudes between 1500 and 1150 m and has mobilized the area marked as Unit 1 in Fig. 2a. The slip plane was formed in highly fractured beds of the Tor Formation, composed here of a combination of

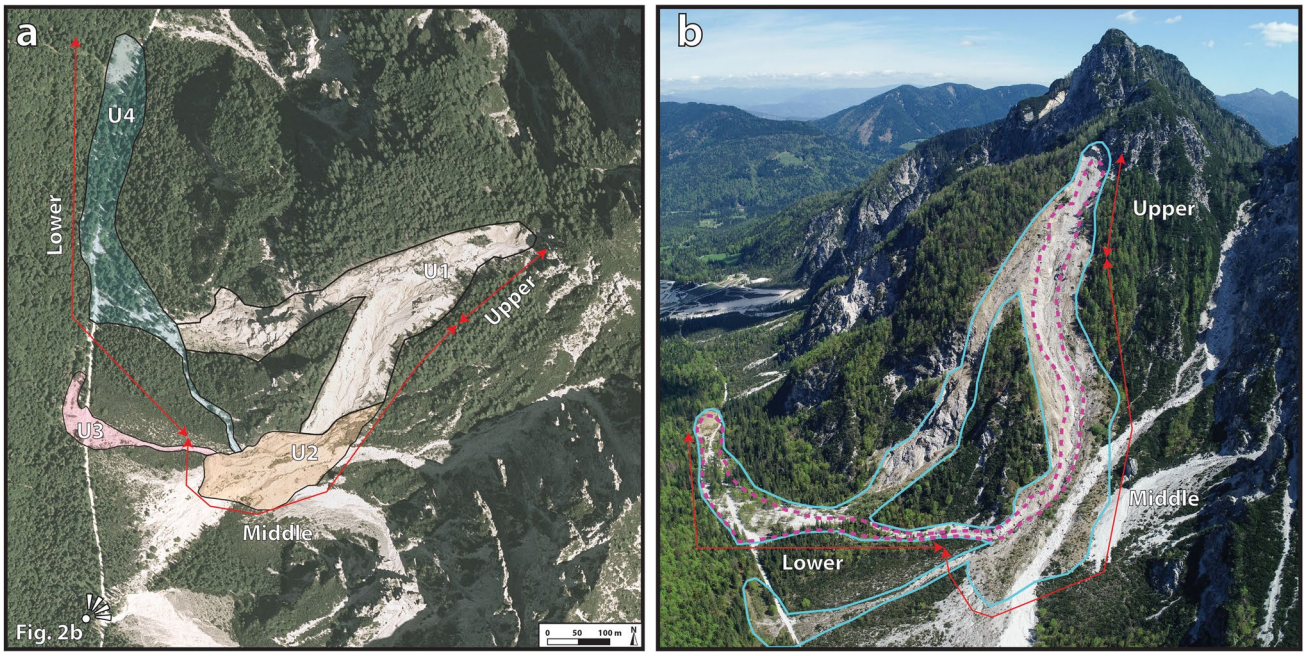

Fig. 2 The Ciprnik complex landslide. **a** Transport-depositional stages of the complex Ciprnik landslide triggered in November 2000 following Šmuc et al. (2015). See text for explanation. The area of the 2023 event is simplified into upper (triggering), middle (transportational), and lower (depositional) parts. **b** Panoramic view at the Ciprnik complex landslide. Light blue line delineates the 2000 event, and violet dashed line delineates the 2023 event

carbonates (limestone, dolomite, and marly limestone) and fine-grained clastic rocks (siltstone, claystone, and marlstone). Bedding is dipping parallel to the slope surface with the dip angle from 25° to 40°. The high monthly rainfall (613.6 mm in November 2000, compared to a monthly average of 159 mm) saturated fine-grained and fractured rock layers, which lead to the translational slip. The slip surface is today covered with large quantities of loose sediment and very little to no vegetation. The initial translational landslide transformed into a debris flow, which travelled and deposited further down the valley between 1150 and 1096 m altitude. The majority of the debris flow deposited in the form of up to 5 m tall debris-flow lobe (Unit 2 in Fig. 2a) over the alluvial fan. This lobe was further eroded by two debris flows that followed shortly after (probably within hours) the deposition of Unit 2 (Units 3 and 4 in Fig. 2a). Unit 3 travelled as a smaller debris flow further west towards the road and valley floor and stopped at an approximate altitude of 1045 m. Unit 4 is characterized by a channel in the upper part, which was a few 10 s of metres wide, 300 m long and cut into a few 10 s of meters into Unit 2 and older deposits. The central part of Unit 4 stretches from the channel mouth at 1060 m down to approximately 1013 m. The central part is 470 m long and up to 140 m wide and is characterized by deposition of a poorly sorted coarse-grained fan-shaped sedimentary body. The surface inclination of the central part decreases gradually from 20° at the channel mouth down to 5° at the lower reaches. The fan-shaped sedimentary body of the central part of Unit 4 is also characterized by a downward increase in fine-grained sediment. The terminal part of Unit 4 is therefore characterized only by sand and mud fraction, which are forming a swampy area measuring approximately 7000 m^2 at altitudes between 1013 and 1010 m. The 2000 event did not result in any casualties and caused relatively little damage to the infrastructure. The only affected infrastructure was a gravel road leading towards the Tamar mountain hut, which is closed for vehicles. It is, however, a popular route for tourists and hikers, but none were present in the area at the time of sliding. A large section of the road was completely buried for several days but suffered no major damage. Until the material was removed from the road, an alternative, undamaged road was used to reach the mountain hut.

For the purposes of this study, we simplified the segmentation of the whole area affected by the Ciprnik landslide into the upper part where the landslide was triggered, the middle part where predominantly transportation occurred, and the lower part where predominantly deposition occurred (Fig. 2b).

Methods

Photogrammetric surveying

We produced a time series of high-resolution digital elevation models (DEMs) with structure-from-motion photogrammetry, using two sources of photographs: (1) high-altitude nadir aerial photographs acquired in regular national topographic surveys by the Surveying and Mapping Authority of the Republic of Slovenia (GURS), and (2) our own UAV surveys.

Aerial photographs were acquired in years 2006, 2011, 2015, 2017, and 2020. Flying altitude was around 5.500 m a.s.l., each photo covering the ground area of approximately 3.8 × 2.5 km. A different camera was used in each epoch (except in 2017 and 2020 when the same camera sensor was used), and consequently, the image resolution ranges from 106 Mp (epoch 2006) to 340 Mp (epochs 2017 and 2020). Direct georeferencing, using precise camera coordinates and

orientation parameters supplied by GURS, was used to georeference this dataset. To adequately cover the study area, 6–9 aerial images were used per survey epoch.

We performed surveys with the DJI Phantom 4 RTK UAV in years 2020 (27. 11. and 30. 11.), 2021 (22. 11.) and 2023. In 2023, two surveys were conducted, immediately after the 24. to 25. 10. landslide reactivation: on 26. 10. and on 7. 11. Surveys were performed with pre-programmed flight missions following an inclined plane, approximating the general orientation of the ground slope. To optimally cover the terrain shape, the study area was divided into four overlapping survey mission areas. The UAV was flying at a distance of 100 m from the reference plane, providing a nominal ground sampling distance of 2.74 cm per pixel. Survey photos were acquired with two look angles: perpendicular to the reference plane (ground) and in nadir orientation. UAV photos were directly georeferenced with the post-processed kinematic method in Emlid Studio v1.6 software, using the raw GNSS observations from the drone and from our own GNSS field base station, both recording multi-frequency and multi-constellation data. The precise absolute position of the GNSS base was obtained with static processing in Emlid Studio, using the RINEX reference data of the Slovenian national permanent GNSS network SIGNAL. An exception in the UAV time series is the 26. 10. 2023 survey, which was performed to rapidly assess the situation after the landslide reactivation, using the DJI Mavic 2S UAV by manual piloting. This UAV does not record raw GNSS observables, and therefore, obtaining precise locations of photographs with post-processing was not possible.

Photogrammetric reconstruction was performed with Agisoft Metashape Professional v2.0 software. The two datasets, GURS aerial photographs and UAV photographs, were processed separately. In the first step, georeferenced photos from all survey epochs were aligned together, and alignment was iteratively optimized to reduce alignment errors. Then, a point cloud was generated for each survey epoch. Finally, DEMs were produced from point clouds, and orthomosaics were generated from photos using DEMs as the reference surfaces. Resolution of UAV-derived DEMs ranges from 11.5 to 16.3 cm, whereas the aerophoto-derived DEMs have a resolution of 50 cm.

The produced DEMs and orthomosaics were analyzed in the QGIS software (QGIS 2021a) to detect surface changes. Changes were detected visually in computed DEMs of difference (DoDs) and in the orthophotos of each survey. DoDs were computed following the methodology of Wheaton et al. (2010) and Westoby et al. (2012). Calculation of volumetric changes was done by using the QGIS Volume calculation tool plugin (QGIS 2021b), and the amounts were obtained in cubic metres with a precision of 0.1 m^3. Interpretation was aided by visual inspection of orthoimagery to assess the geomorphic changes. Because the areas of complex landslide activity include densely vegetated areas, we employed several filtering techniques to recover ground point data from below vegetation, but we found that only a very limited number of ground points could be obtained, which is a known limitation of photogrammetric point clouds (e.g. Sestras et al. 2025). Therefore, we limited the volumetric calculations to areas devoid of vegetation, which we manually delimited with polygons in QGIS. Only in the case of the October 2023 event do we provide an estimated volume of sediment deposited in the lower vegetated area. The estimation is based on the vegetated surface area and the estimated thickness of deposited sediment.

Sedimentary analysis and meteorological data

Fourteen samples CP 1 to CP 14 were taken in the transport-depositional area of the 2023 event (Fig. 6). Numbering of samples reflects their distance from the triggering area, with CP 1 being most proximal and CP 14 being most distal. Samples CP 1 and CP 2 were taken from a debris-flow levee, while the remaining samples CP 3 to CP 14 were taken from the depositional area of the debris flow. Additional coarse-grained sample DL2000 was obtained from the debris-flow lobe of the 2000 event for a comparison to the 2023 event.

Samples CP 1 to CP 10 are coarse grained (containing clasts measuring up to very coarse gravel) and were first sieved using standard sieve pans with diameters ranging from 1 to 32 mm. Clasts larger than 64 mm were measured manually, and particles smaller than 1 mm were measured using the Fritch Analysette 22–28 particle sizer with laser granulometry and dynamic image analysis. Sieving and particle sizer measurements were combined into a single measurement per site. Samples CP 11 to CP 14 were sampled from fine-grained hyperconcentrated-flow deposits, for which the granulometric analysis was performed using above-mentioned particle sizer.

Meteorological data was used to interpret rainfall conditions that triggered the events and caused surface changes (Fig. 3). They were obtained from the Rateče meteorological station operated by Slovenian Environment Agency (ARSO 2023). Data is openly available and offers daily rainfall values that are measured each day at 7:00 a.m. local time. Additionally, temperature and rainfall measurements in 30-min intervals are also available for the 2023 event and were interpreted as well. The Slovenian Environment Agency defines an intense rainfall event as a 24-h rainfall that exceeds 50 mm (ARSO 2006). Such events occur eight to ten times per year at the Planica valley (ARSO 2006, 2021a, b). We used the ARSO (2006) definition of intense rainfall as a rainfall value that potentially can trigger a landslide, which is also in line with values for landslide triggering by Guzzetti et al. (2007). We checked the meteorological records to detect any potential triggering rainfalls that occurred between each aerial survey and determine their statistical return periods according to ARSO (2025). We then interpreted the volume and extent of surface changes in accordance with rainfall events. We also identified months in which long-duration rainfall exceeded average monthly rainfall for 100% or more (ARSO 2021a, Fig. 1b). Months and days where precipitation occurred as snow were excluded from the analysis.

Results

Surface changes between 2000 and 2020 based on GURS derived aerophotography

Slope movement activity in the period between 2006 and 2020 was determined using DEMs generated from GURS aerophotographs (Figs. 4 and 5). Surface changes were analyzed in the upper and middle parts of the landslide area, whereas the lower area, where predominantly deposition occurs, was excluded due to dense vegetation cover. Consequently, the calculated volumes of the

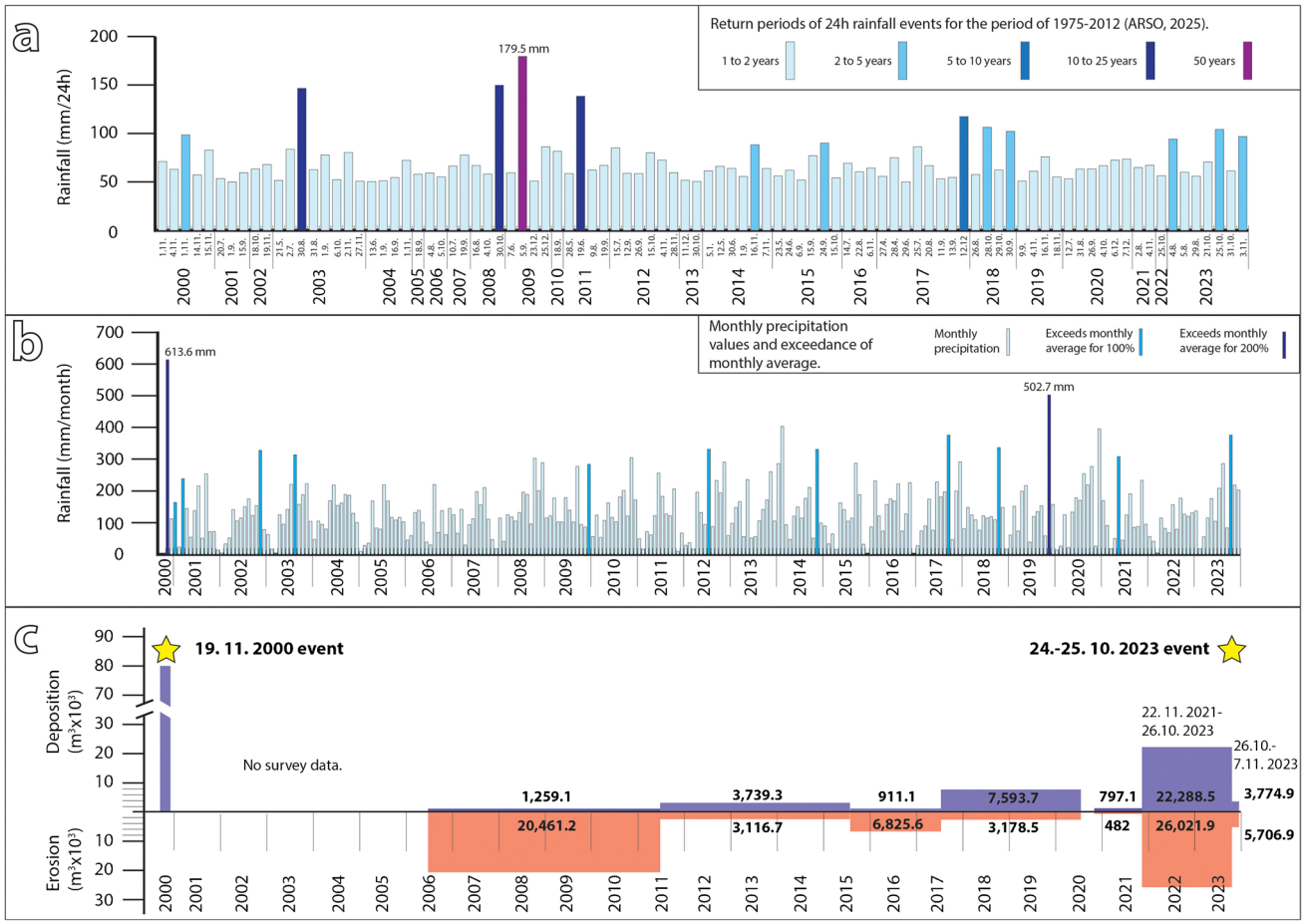

Fig. 3 Schematic overview of rainfall events and volumes of deposited and eroded material. **a** In total, 94 intense rainfall events with different return periods occurred in between the 2000 and 2023 events. **b** 11 months exceeded the monthly rainfall average for 100%, and 1 month exceeded for more than 200% (November 2019). **c** Volumetric surface changes between each survey. The 2000 event measured approximately 80,000 m^3 (Komac and Zorn 2007), approximately four times larger than the October 2023 event

transported and deposited sediment refer to the landslide upper and middle parts only (Figs. 2 and 3).

The most extensive changes occurred in the period between 2006 and 2011 (Figs. 3c and 4a); 20,461.2 m^3 of sediment was eroded and 1259 m^3 of sediment deposited. In this period, a more than 3 m deep torrential channel was formed (Figs. 4a and 5a), extending from the middle part of the slip surface to the bottom of the valley, where sediment was deposited on a fan-shaped surface (Unit 4 of Šmuc et al. 2015). The erosion was predominantly manifested by minor landslides and slumps of loose material that remained on the slip surface after the 2000 event. The formation of the torrential channel was facilitated by several intense rainfall events following the 2000 event (Figs. 3 and 5a). Between the 2000 event and 2006, there were 4 months in which the average monthly rainfall was exceeded by more than 100% (Fig. 3b). In the same time period, 20 intense rainfalls, predominantly with a return period of 1 to 2 years, occurred. One intense rainfall with 146.5 mm and a return period of 10 to 25 years occurred on 30. 8. 2003 (Fig. 3a). Between 2006 and 2011, there was only 1 month in which the monthly rainfall average was exceeded by more than 100%, and 14 intense rainfalls occurred. Two of them had a return period of 10 to 25 years. The rainfall event of 5. 9. 2009 (return period of 50 years; 179.5 mm) was a record-breaking 24-h rainfall event in the entire period from the beginning of meteorological observations (ARSO 2021a).

In the subsequent period between 2011 and 2015, the volume of deposited and eroded material was 3739.3 m^3 and 3116.7 m^3, respectively (Fig. 3c). Most of the erosion occurred in rills and gullies tributary to the main torrential channel (Figs. 4b and 5b). Deposition occurred mainly in the torrential channel and in areas where, in previous years, erosion occurred. The mass-movement processes were limited to smaller slumps and slidings of loose material (Fig. 5b). In this period, 2 months exceeded the monthly rainfall average by more than 100% (July 2012 and November 2014) and 20 intense rainfalls occurred. Two had a return period of 2 to 5 years, while the rest had a return period of 1 to 2 years (Fig. 3).

Erosion was much more extensive in the period between 2015 and 2017, with 6825.6 m^3 of eroded sediment and only 911.1 m^3 of deposition (Figs. 3c and 4c). In the upper and middle parts, erosion predominantly occurred in rills and gullies, and the main torrential channel was also deepened. A few erosional events can be attributed to slumps (Figs. 4c and 5c). One month (September 2017) exceeded the monthly rainfall average by more than 100%,

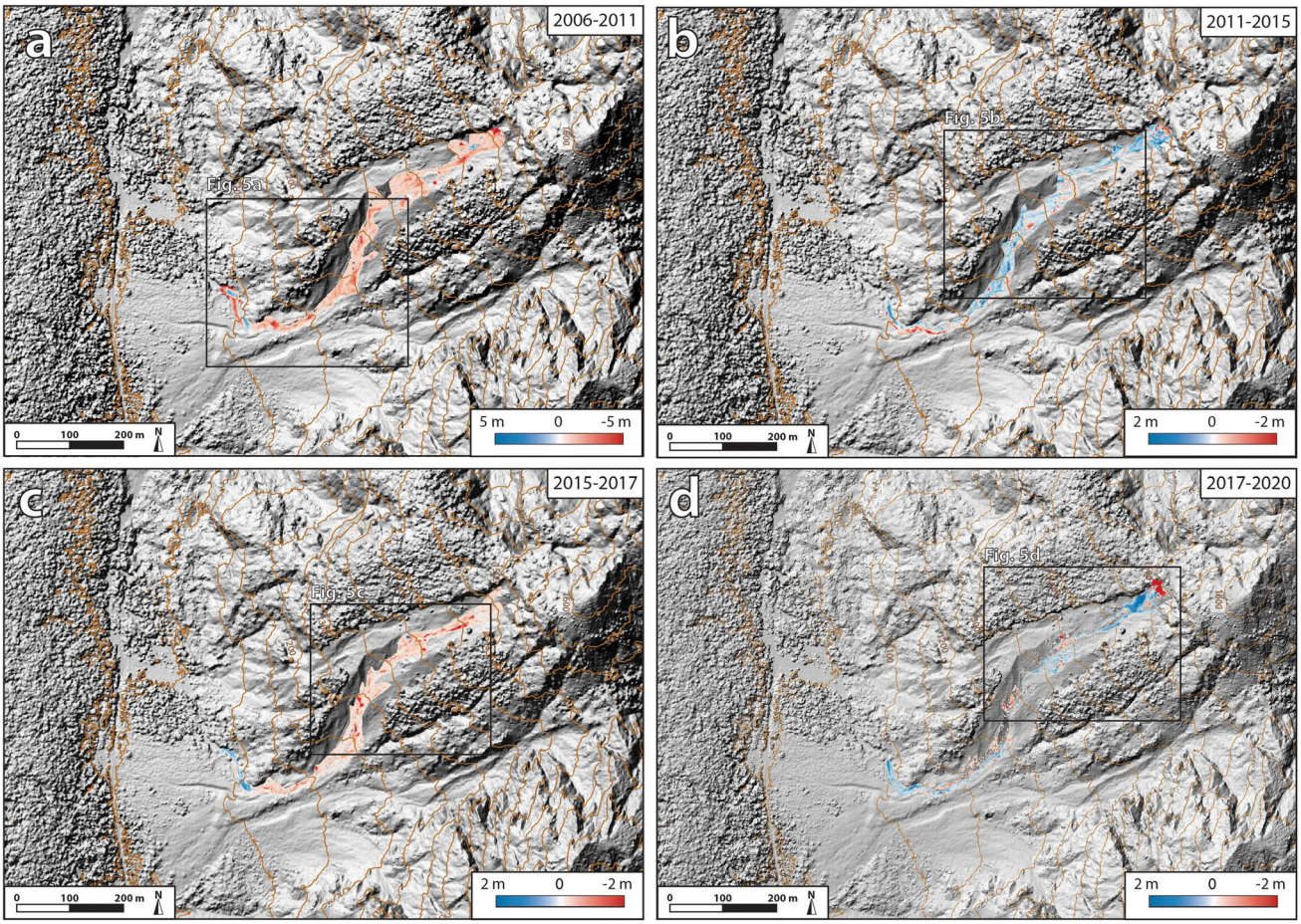

Fig. 4 Surface changes following the complex Ciprnik landslide in the period of 2006 to 2020. **a** Surface changes in the period between 2006 and 2011 when erosion was most dominant. Several minor landslides and slumps of loose material occurred and formation of a torrential channel. **b** In the period between 2011 and 2015, erosion occurred in rills and gullies tributary to the torrential channel, while deposition occurred predominantly in the torrential channel. **c** In the period between 2015 and 2017, erosion predominantly occurred in rills and gullies in the upper and middle parts, while the torrential channel was deepened. **d** In the period between 2015 and 2020, the major changes occurred in the upper part where a landslide deposited. The remaining erosion and deposition occurred in rills, gullies, and in the torrential channel

and 11 intense rainfalls occurred. One had a return period of 5 to 10 years (12. 12. 2012; 117.4 mm), and the rest had a return period of 1 to 2 years (Fig. 3a and b).

In the period between 2017 and 2020, deposition was again more pronounced, with 7593.7 m^3 of deposited sediment and 3178.5 m^3 of erosion (Figs. 3c and 4d). The major changes occurred in the upper part, where a landslide mobilizing 1972.2 m^3 of material occurred (Fig. 5d). The mobilized material was deposited in the upper part as unconsolidated sediment. The remaining erosion and deposition occurred separately in rills, gullies, and in the torrential channel (Figs. 4d and 5d). In this period, 1 month exceeded the monthly rainfall average by 100%, and one for more than 200% (November 2019), while there were 12 intense rainfalls with a return period of 1 to 2 years and 2 intense rainfalls with a return period of 2 to 5 years (Fig. 3a and b).

Surface changes between 2020 and 2021

UAV-derived DEMs covering the period from 2020 to 2021 (surveys were taken on 27.11. 2020, 30.11. 2020 and 22.11. 2021) indicate only minor changes on the surface of the Ciprnik landslide: 797.1 m^3 of sediment was deposited and 482 m^3 eroded (Table 1). In the upper part, two rock avalanches measuring 155.8 m^3 and 33.3 m^3 occurred in highly fractured Conzen dolomite (Figs. 6a and 7a). The mobilized material of both events deposited in the gullies in the upper part. In the middle and lower parts, erosion and deposition occurred due to the activity of the torrential channel. In the 2020–2021 period, between the consecutive surveys, six intense rainfalls with a return period of 1 to 2 years occurred (Fig. 3). Of those, two daily rainfalls exceeded 70 mm (6. and 7. 12. 2020), three daily rainfalls exceeded 60 mm of rainfall (12.

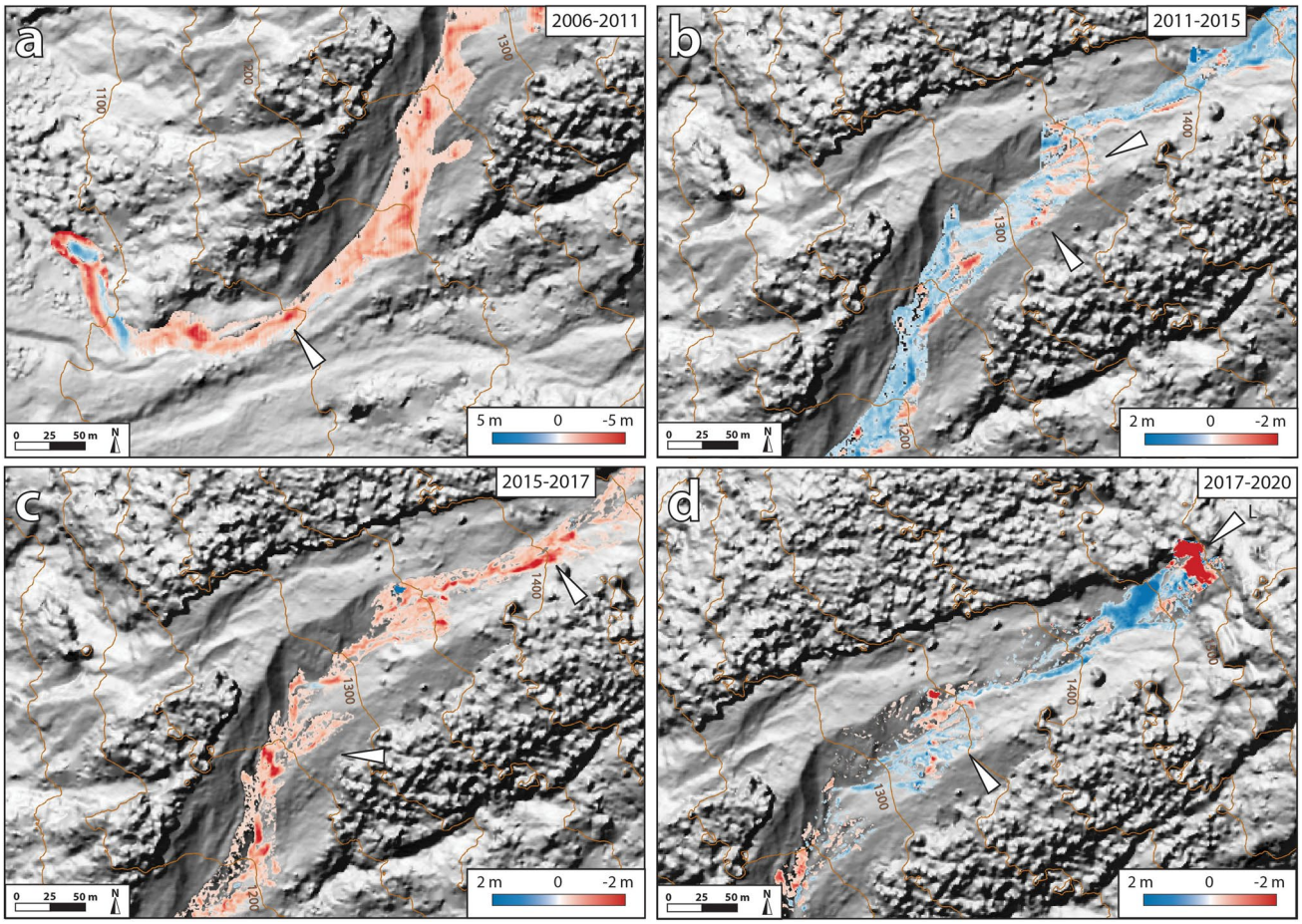

Fig. 5 Details of the surface changes in the period of 2006 to 2020. **a** Area where an up to 3 m deep torrential channel was formed marked by a white arrow. **b** Formation of erosive rills and gullies tributary to the torrential channel marked by white arrows. **c** Several slumps, rills, and gullies marked by a white arrow were formed in the period 2015 and 2017. **d** In the upper part, a small landslide marked by a white arrow (L) measuring 1972.2 m^3 occurred. Additional erosion and deposition occurred in rills, gullies marked by a white arrow and in the torrential channel

10. 2020, 3. 5. 2021 and 2. 8. 2021), and one daily rainfall exceeded 50 mm (12. 10. 2020) (ARSO 2023). In May 2021, the monthly rainfall average was exceeded for 100% (Fig. 3).

Major reactivation event of October 2023

Reactivation of complex landsliding was triggered by heavy rainfall on the night from 24. to 25. 10. 2023, according to credible social media reports by the Mountain Rescue Association of Slovenia and meteorological data (ARSO 2023). Continuous rainfall started in the morning of 24. 10. at 9:00 AM local time and lasted until early morning of 25. 10. at 5:00 AM local time, totalling 104.2 mm of rainfall. The most intense 30-min rainfall intervals occurred at 12:00 and 19:30 on 24. 10., amounting to 4.8 and 5.8 mm, respectively. According to ARSO (2025), rainfalls of the magnitude of the 24. to 25. 10. event have a statistical return period of 5 years.

Surface changes were detected based on comparison of UAV surveys from 2021 and 2023. We conducted the initial UAV survey on 26. 10., one day after the event. The event exhibits all the characteristics of a complex landsliding movement that can be classified as translational slip-debris flow-hyperconcentrated flow event (Fig. 6b). In total, 22,288.5 m^3 of sediment was deposited and 26,021.9 m^3 eroded (Fig. 3, Table 1). In the upper part of the landslide, the movement initiated as a translational slip movement on a planar surface of the Tor formation bedding planes and as a collapse of a rockface composed of Conzen dolomite (Figs. 6b and 7b). This initial landslide measured almost 16,000 m^3. Only a small amount of sediment was deposited there. In the middle part, the triggered material travelled as debris-flow, causing deposition and erosion of sediment. Debris flow was mostly confined to the torrential channel and followed a sinusoidal path. It had the same transport-depositional path as the debris flow of the 2000 event. Sediment of the debris-flow was deposited in form of levees along the transport path (Figs. 6b and 8a). Erosion was severe in the torrential channel, which at some parts was deepened for more than 5 m (Figs. 6b and 8b and c). Up to 1-m-tall levees formed largely at outer banks of the transport path, while erosional cuts formed in the inner banks (Fig. 6b). In the lower part, erosion was minor (228.5 m^3), whereas deposition amounted to more than 12,000 m^3 of sediment in a thickness of up

Table 1 Volumetric changes based on UAV data for the period between 2020 and 7. 11. 2023. *Approximately 6000 m^3 additional sediment was deposited in areas densely vegetated

	27.11., 30.11. 2020–22.11. 2021	22. 11. 2021–26.10. 2023	26.10.–7.11. 2023
Upper part			
Deposition (m^3)	333	1548.2	299
Erosion (m^3)	216.6	15,942.7	321.6
Middle part			
Deposition (m^3)	249.9	8038.6	976.7
Erosion (m^3)	216.8	9850.7	5366.6
Lower part			
Deposition (m^3)	214.2	12,701.7*	2499.2
Erosion (m^3)	48.6	228.5	18.7
Total deposition (m^3)	797.1	22,288.5	3774.9
Total erosion (m^3)	482	26,021.9	5706.9

to 1 m (Figs. 6b and 8d). The actual amount of deposited sediment is larger, however, since for parts of the depositional area, DoDs could not be reliably calculated due to dense vegetation (Figs. 2 and 6b). We estimate that another 6000 m^3 of sediment was deposited there, based on the vegetated area surface (approximately 6000 m^2) and average sediment thickness (up to 1 m). This estimation is in line with the total amounts of sediment eroded by the complex landslide (Table 1). Sediment was highly saturated (Fig. 8d and e), to the extent that it was impossible to stand on it (Supplementary material 1). In the most distal and least inclined part of the landslide, debris flow transitioned into a hyperconcentrated flow. Sediment of hyperconcentrated flow was deposited on a surface area of approximately 4000 m^2 in thickness ranging from a few cm to a few 10 s of cm (Fig. 8e).

Following the main event of the 24. to 25. 10. 2023, heavy rainfall occurred during the next 2 weeks, with the most intense events occurring on 31. 10. and 3. 11. with 61.5 and 96.8 mm of rainfall in 24 h, respectively (Fig. 6d). The rainfall event of 31. 10. had a return period of 1–2 years, while the rainfall on 3. 11. had a return period of 2–5 years (Figs. 3 and 6d). We therefore performed a new UAV survey on 7. 11. 2023. We find that very little erosion or deposition occurred in the upper part of the landslide area, with only a few 100 m^3 of sediment eroded and deposited. Erosion was much more pronounced in the middle area, with more than 5000 m^3 eroded material removed mainly from the torrential channel banks and by deepening of the channel (Figs. 6c and 7c and d and Table 1). Evidently, the heavy rainfall subsequent to the main event did not cause any major triggering in the upper part of the landslide (Figs. 6c and 7c). Some minor slides and slumps did occur in the middle part, but the main effect of the rainfall was to wash and erode the sediment in the torrential channel (Figs. 6c and 7d). The lower area was dominated by sediment deposition by water flow (Fig. 6c). Again, due to the dense vegetation, the calculated amount of deposits is underestimated. We estimate that another few 100 m^3 were additionally deposited. We conclude that processes occurring in the depositional area after the main 2023 event cannot be regarded as typical mass movements but rather as water-flow-driven sediment transport and deposition.

Sedimentary analysis

All coarse-grained samples (CP 1 to CP 10) exhibit sedimentary texture of mud-sandy-gravel (Fig. 9). However, the granulometric analysis shows that relative percentages of mud (combined silt and clay), sand, and gravel fraction vary significantly, with a clear trend of fining of the sediment downward from the initial sliding area. This was also clearly visible in the field survey, which revealed that larger clasts (boulders and cobbles) were deposited in the upper part, medium clasts (pebbles, sand, and mud) in the middle part, and fine-grained sediment (fine sand and mud) in the distal parts (Fig. 8).

Two samples from the highest part of the sampling area (CP 1 and CP 2), taken from the debris-flow levee, contain the highest percentage of gravel (76.2% and 77.8%, respectively). CP 1 had a slightly lower amount of mud (7%) and a higher amount of sand (16.8%) compared to CP 2 (10% of mud and 12.2% of sand). In samples CP 3 to CP 10, the proportion of gravel gradually decreases and remains below 70%, except for sample CP 5 (71.7%). Sample CP 10, the most distal sample of the samples CP1 to CP10, contained only 39% of gravel. Consistent with that, the proportion of sand and mud significantly increases towards the distal part of the area, with the lowermost sample CP10 containing the highest percentage of sand (44.9%). Sample CP 1 had the least amount of mud, and samples CP9 and CP10 had the most (16.4 and 16.1%, respectively).

Downward fining is clearly present also in the fine-grained samples CP 11 to CP 14 (Fig. 10), obtained from the most distal part of the hyperconcentrated flow in a profile of 80 m in length. Sample CP 11 belongs to the group of silty sand, whereas the other three belong to sandy silt. The amount of clay, silt, and sand varies between the samples (Fig. 8). The amount of clay fraction increases from 3 to 13%, and the amount of silt increases from 37 to 59%. The amount of sand decreases from 60 to 28%. Sample DL2000, taken from the depositional lobe of the 2000 event, belongs to the textural group of muddy gravel, containing 19.1% of mud, 14.9% of sand, and 65.9% of gravel (Fig. 9).

Effects on infrastructure and environment

The effects of the 2023 complex landslide were predominately on the natural environment, with some effect on infrastructure (Fig. 8). Deposited sediment buried approximately 400 m long section of the gravel road leading to the Tamar mountain hut, up to 1 m in height. Because the sediment was highly saturated (Supplementary material 1), the road was closed for several weeks before it could be cleaned and reopened. The deposited sediment, however, did not cause major damage. Power poles located parallel to the road

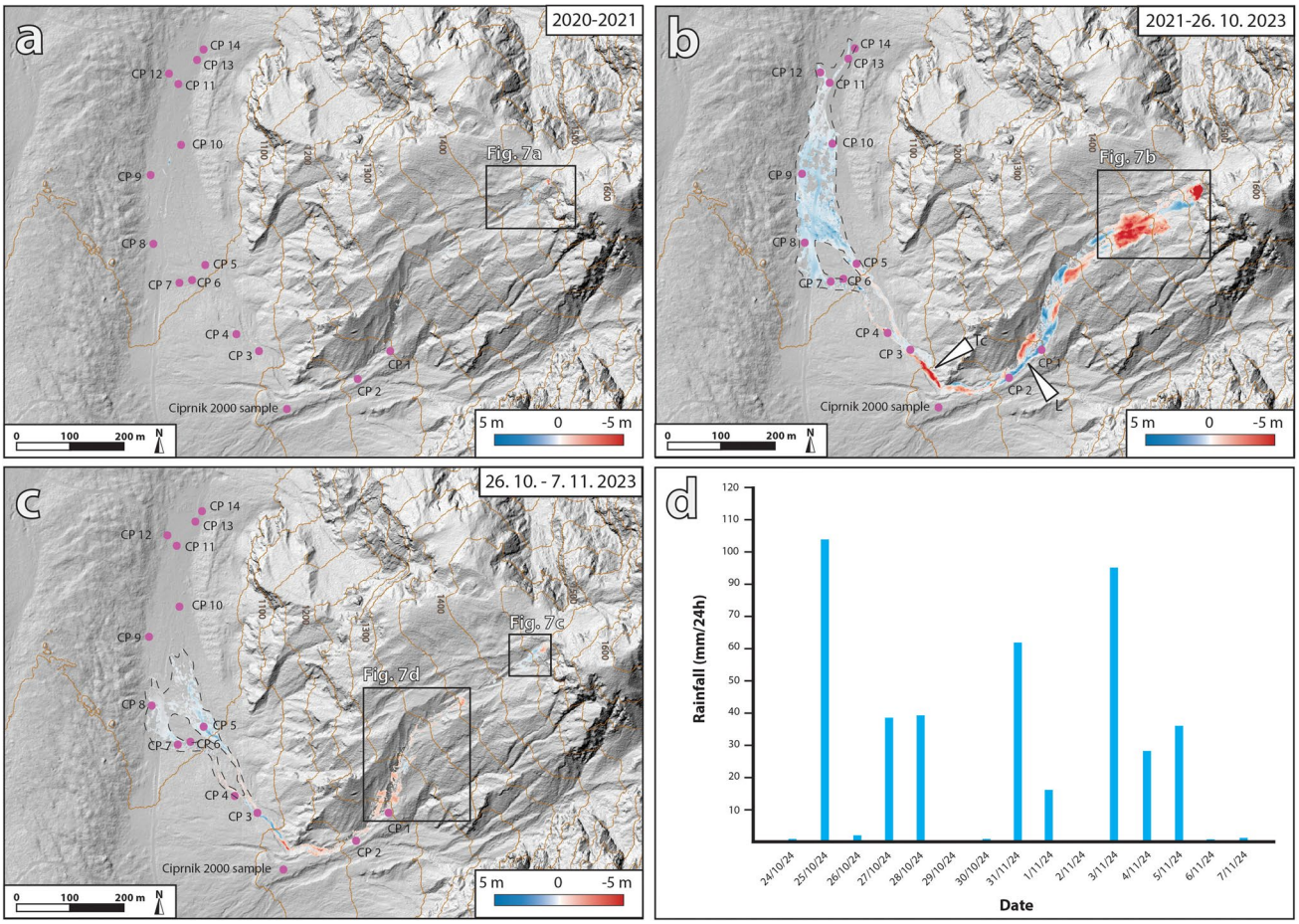

Fig. 6 Surface changes detected in the period between 2020 and 7. 11. 2023 and rainfall data for the period between 24. 10. and 7. 11. 2023. **a** Two minor rock avalanches occurred in the upper part, while some erosion and deposition occurred in the torrential channel. **b** The 2023 event. Deepening of the torrential channel (Tc) and debris-flow levees (L) are clearly visible in the DoD image. Dashed line delineates the area of deposition. **c** Subsequent erosion and deposition of sediment as a result of additional rainfall between 24. 10. and 7. 11. 2023. Dashed line delineates the area of deposition. **d** Daily rainfall amounts (mm/24 h) between 24. 10. and 7. 11. 2023

were only partly buried and did not suffer any mechanical damage (Fig. 8d).

The major effects on the environment were extensive erosion and deposition of sediment on the slopes of Ciprnik Mountain and at the valley floor. Total erosion and deposition were the largest since the 2000 event. Extensive translational slips reshaped the slopes of Ciprnik Mountain and made it prone to future sliding. Debris flow caused a deepening of the preexisting torrential channel for up to 5 m.

The complex landslide had affected trees predominantly by uprooting and partial burial (Fig. 8c, d, and f). In the area of erosion (area of translational sliding and channel deepening), trees were uprooted or suffered severe mechanical damage. Trees growing on the depositional area were only partly buried (approximately up to 1 m high) and did not withstand major mechanical damage since no scars were visible on the tree bark, regardless of the tree's age and size (Fig. 8d and f). Partially buried trees, however, will experience suppressed growth in the future. In addition, trees growing on the depositional area offered some protective function since there were cases of trees stopping several large boulders (Fig. 8f). This further indicates that the speed of moving material in the lower parts was not very fast.

Discussion

The major 2000 and 2023 complex landslide events exhibit close similarities in triggering, transport, and depositional characteristics: (1) both are translation slip-debris flow-hyperconcentrated flow events; (2) both events initiated as translational landslides triggered on the bedding-parallel steep plane in highly fractured beds of the Tor Formation; (3) both landslides transformed into debris flows, which were deposited in the same area. However, in the 2023 event, no tall debris-flow lobe formed at the bottom of the landslide, which we attribute to the fact that the 2023 debris flow was channelized into the preexisting torrential channel. The 2023 debris flow instead deposited in a fan shape in the valley bottom at the same location of the 2000 event and eventually transformed

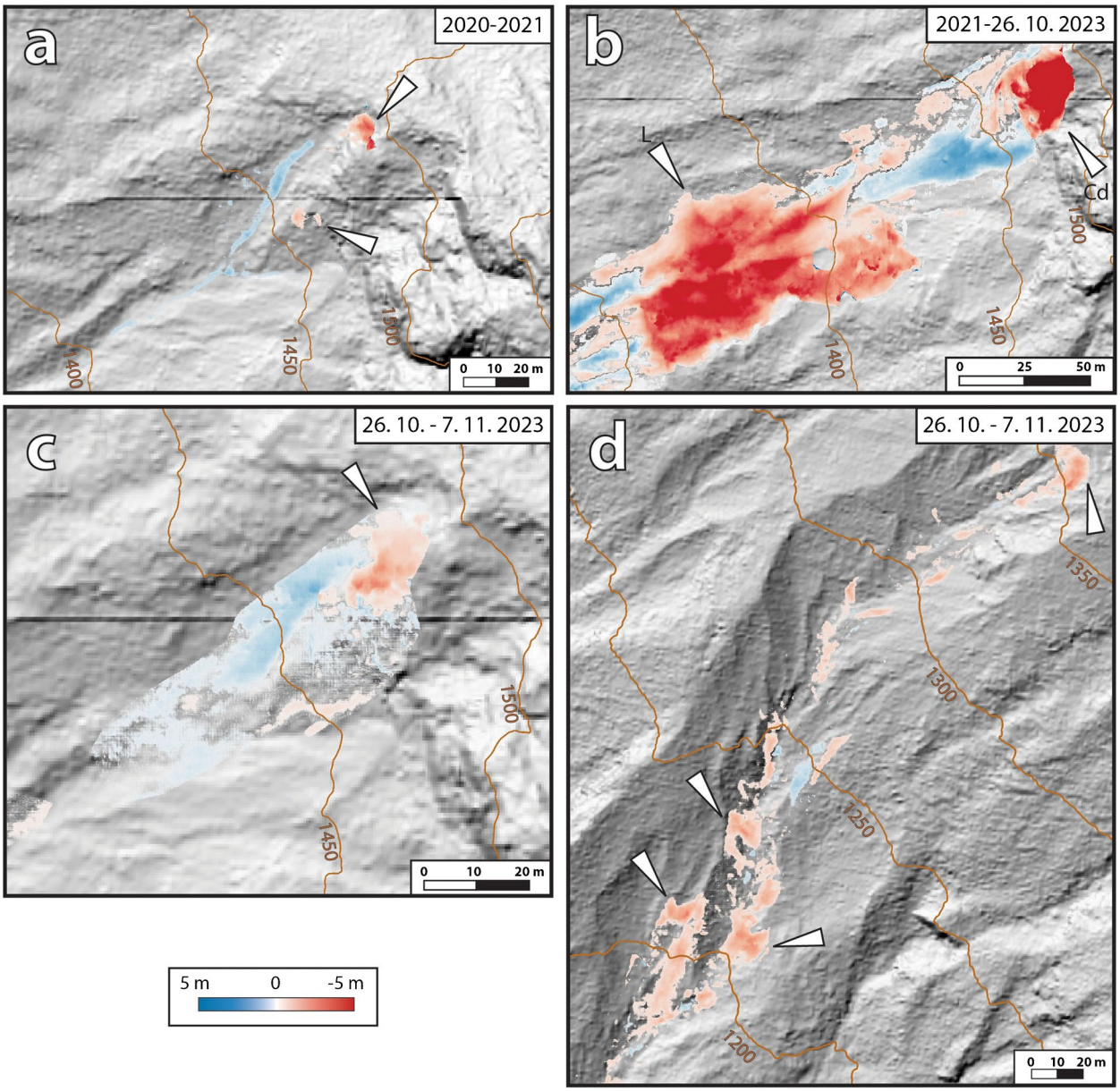

Fig. 7 Details of the surface changes in the period of 2020 to 7. 11. 2023. **a** Two minor rock avalanches marked by a white arrow that occurred in highly fractured Conzen dolomite. **b** The initial landslide that occurred on a planar surface of the Tor formation layers (L) and as a collapse of a rockface composed of Conzen dolomite (Cd) marked by white arrows. **c** Minor sliding marked by a white arrow that was limited to the upper part of the complex landslide. **d** Some minor slides and slumps marked by white arrows, which were predominantly washed into the torrential channel by rainfall

into hyperconcentrated flow that was deposited in the terminal part of the landslide. In both events, the entire process of sediment fining from muddy-sandy-gravel to sandy-silt occurred over a travel distance of approximately 500 m. The granulometric analysis shows that the 2000 event had a higher amount of fines than the 2023 event. Higher content of fines in the 2000-event deposits could be attributed to the mechanical weathering of the clasts. A sample was taken from the debris flow lobe that remained stable for more than two decades, and a higher quantity of fine grains could collect over time (c.f. Hooke 1993).

The crucial difference between the 2000 and 2023 events is in the triggering mechanism. The 2000 event was caused by prolonged water accumulation during record-breaking rainfall that saturated fine-grained and fractured rock layers. Cumulative rainfall prior to the 2000 event was 228.3 mm in 7 days and 356.7 mm in 14 days (Šmuc et al. 2015). The 2023 event was instead triggered by

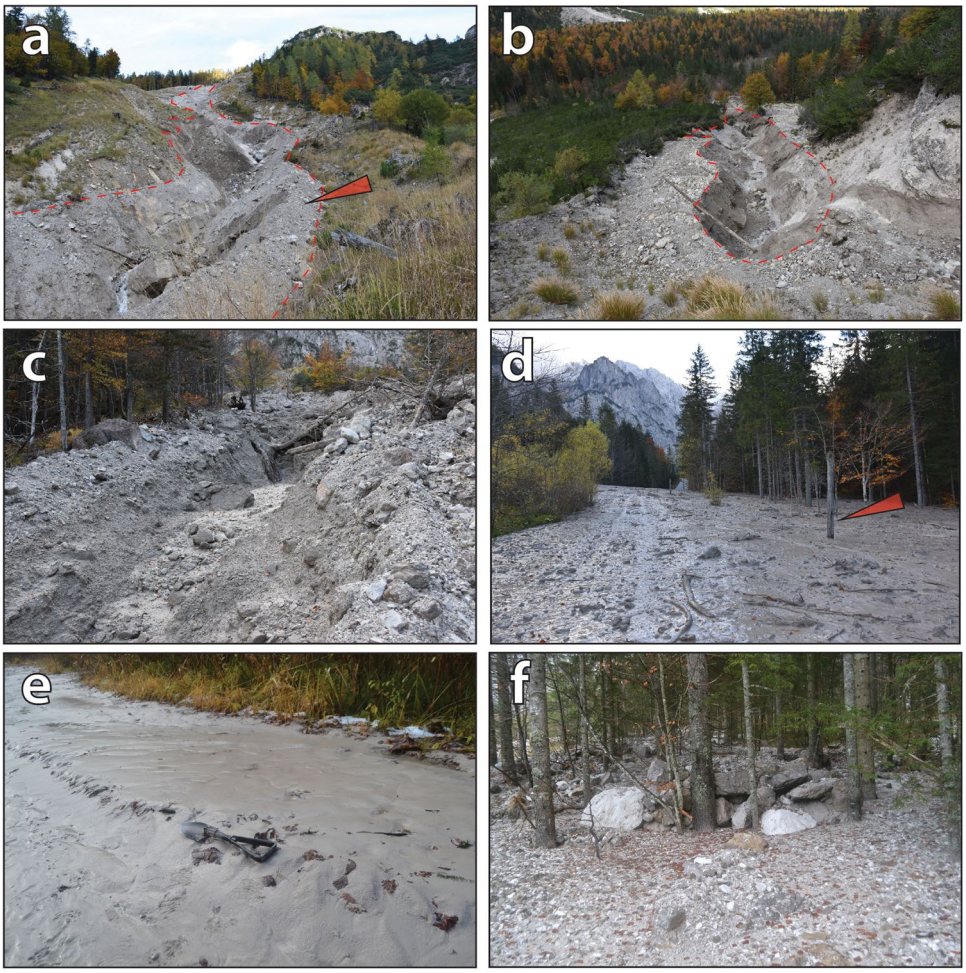

Fig. 8 Characteristics of the 2023 event photographed a day after the event (26. 10. 2023). **a** View towards middle transportational (red dashed line) part of the Ciprnik complex landslide. Levees where samples CP 1 and 2 were taken are clearly visible (red arrow). **b** In the transportational part, debris flow caused major erosion by deepening the preexisting torrential channel up to 5 m (dashed line). **c** Transition from erosion in the middle part to deposition in the lower part of the 2023 event. Debris flow caused uprooting of several trees. Samples CP 3, 4, 5, and 6 were taken in this area. **d** Lower depositional part of the 2023 event. Sediment was highly saturated with water and had a significantly higher amount of fines (sand, silt, and clay) and a lower amount of cobbles and boulders (comparison to the Fig. 8c). Road leading towards the Tamar hut was covered by up to 1 thick layer of sediment. Trees and electric poles (marked by a red arrow) were not damaged but only partially buried. Samples CP 8, 9, and 10 were taken in this area. **e** A few 10 s of centimetres thick layers of sandy silt deposited in the most distal depositional part of the 2023 event. Samples CP 11 to 14 were taken in such deposits. **f** Trees stopped transported boulders that measured up to 1 m. Sample CP 7 was taken in the frontal area of trees

a short-duration high-intensity rainfall of 104.2 mm in 24 h that is relatively common for the study site. It is likely that the 2023 event would not occur on its own without the occurrence of the 2000 event. The 2000 event was triggered by a record-breaking prolonged rainfall that resulted in movement on slopes highly prone to sliding. Future mass movements are then easily triggered by rainfall events with relatively common rainfall values. Based on this study and remaining material on the slopes of Mount Ciprnik, future events of magnitudes similar to or higher than the 2023 event are possible.

Between the major 2000 and 2023 events, no mass movement of similar magnitudes occurred, despite the occurrence of several potential rainfall triggering events such as record-breaking 24-h rainfall (5. 9. 2009) and high monthly rainfall in November 2019. Rainfall events therefore caused only to wash off the loose sediment and minor slidings (Figs. 3, 4, and 5). The most extensive changes on the landslide surface occurred in the period between 2006 and 2011, closest to the occurrence of the 2000 event, as demonstrated by our 2006–2023 time series of DEMs. Extensive erosion has mobilized the large quantity (more than 20,000 m^2) of unstable sediment left on upper steep slopes, where the 2000 event commenced. This sediment was easily eroded by several intense rainfalls (namely the 5.9. 2009 event) as well as by lighter rainfalls. In the following years, the erosion and deposition were less severe, with a few 1000 m^3 of sediment eroded and deposited per a time span of 3 to 4 years. It is likely that larger amounts of sediment were eroded in

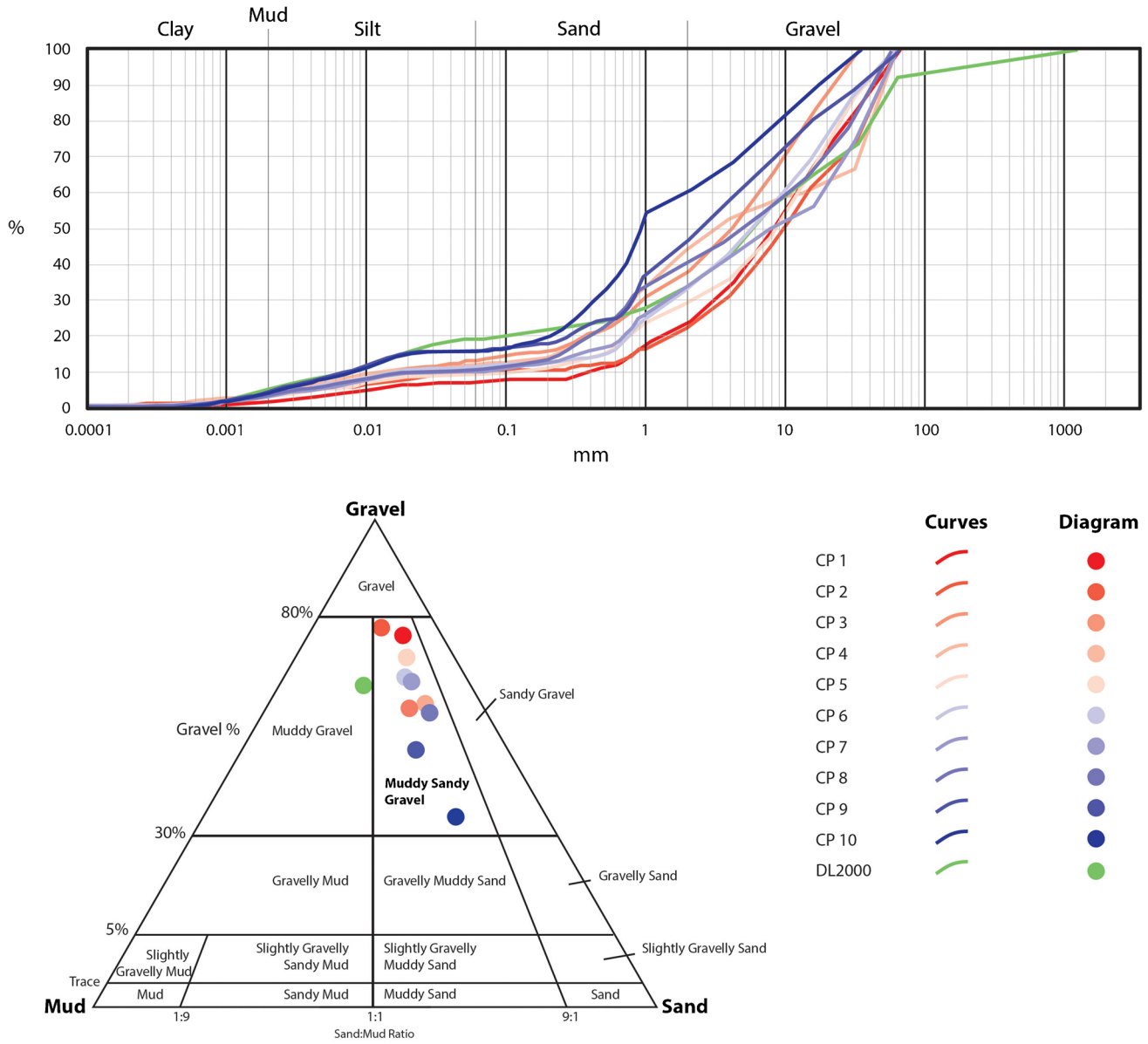

Fig. 9 Granulometry of sampled CP1 to CP 10 and of the sample DL2000 taken from the Ciprnik 2000 event. Ternary diagram clearly shows downward fining of sediment, with the most distal sample (CP 10) having the least amount of gravel

the initial stage after the 2000 event and that the area slowly but not completely transitioned into partial stability. Our 2020–2021 UAV survey confirms that only a few 100 m^3 of erosion and deposition occur on an annual basis. We attribute these 2020–2021 changes to six intense rainfall events in the period 2020 to 2021 that exceeded the threshold of 50 mm of rainfall in 24 h. These events washed off the loose sediment from the unvegetated and steep main sliding surface but did not trigger landslides or slumps. Although a UAV survey was not performed in the year 2022, no major mass movement occurred between 2021 and the event in 2023. The absence of a major movement is confirmed by our field observations and meteorological data. In 2022, no precipitation events exceeding monthly averages occurred, and only one intense rainfall with a 1 to 2 year return period occurred (25. 10. 2022, 56.3 mm, Fig. 3a). Such rainfall was not intense enough to trigger a major mass movement. Surface changes in the year 2022 were most likely similar to the ones in the 2020–2021 surveys, and the changes between 2021 and 2023 can be almost entirely attributed to the 2023 Ciprnik complex landslide event.

The results of this study show that the critical precipitation thresholds for triggering future landslides are highly unpredictable. Firstly, the two triggering precipitation events differ drastically in their duration, intensity, and return periods. Secondly, rainfalls of similar or even higher intensity and duration occurred in 23 years between 2000 and 2023 without triggering any major landslides. These facts, combined with the observed annual surface changes

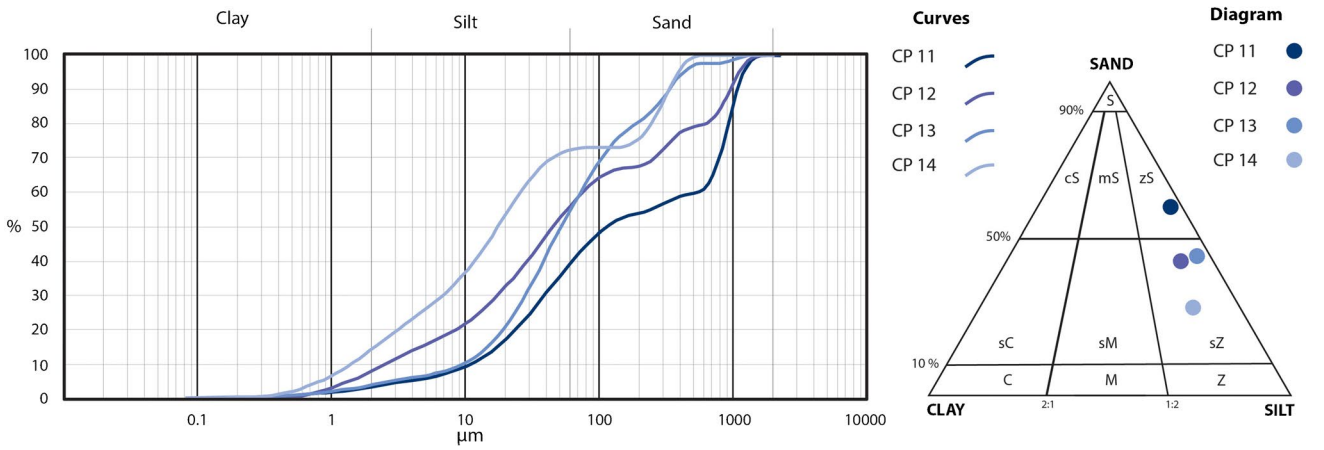

Fig. 10 Granulometry of samples CP 11 to CP 14. Within a very short transport distance, the downward fining is clearly visible

after the 2000 event, clearly indicate that future landslide triggers are more likely to be caused by changing surface conditions in combination with geological structure and heterogeneous lithology rather than by exceeding specific thresholds related to rainfall duration and intensity. This study also clearly demonstrates that large-scale mass movement events at the location of older mass movement deposits can be triggered by relatively ordinary precipitation events.

The Ciprnik complex landslide poses a risk to the gravel road leading to the Tamar mountain hut. In both major mass movement events, the road was blocked for several days until the landslide material was removed. While the road is closed for vehicular traffic, it is heavily used by a large number of visitors. In view of people's safety and the very unpredictable nature of the triggers, we advise the authorities to warn the public of possible landslides during all rainfall events.

Conclusions

The Ciprnik complex landslide triggered in November 2000 is an example of a translation slip-debris flow-hyperconcentrated flow event triggered by long-term accumulation of rainfall. After the event, the slopes remained unstable, with a continuing erosion amounting to approximately a 1000 to 3500 m^3 per year. A major reactivation occurred on the night from 24. to 25. 10. 2023, when a complex landslide mobilized 26,000 m^3 of material. This event had the same transport and depositional characteristics as the initial 2000 event. The sliding started as a translational landslide on steeply inclined, highly fractured bedding planes that are parallel to the slope surface. Sliding material transformed into a debris flow after a short travel distance and was deposited at the valley bottom with approximately 1380 m of run-out horizontal distance and 485 m in vertical direction. Fining down of the deposited sediment was very pronounced, most evidently with the deposition of hyperconcentrated flow composed of sandy silt in the most distal reaches. In both events, each of the three transport and depositional stages of complex landslides had the same effects on the surroundings. The main difference between both events was in the triggering rainfall events. While both events are interlinked to rainfall triggers, the triggering rainfalls drastically differ in their intensity and duration. While the 2000 event was induced by a record-breaking long-duration rainfall lasting for more than 2 weeks, the 2023 event was triggered by a relatively common short-duration (24 h) and intense rainfall event. This study clearly shows the complexity of required trigger conditions in the aftermath of the main mass wasting event. Even in the later events, which have the same transport mechanisms as the original event, the triggering precipitation can differ considerably in duration and magnitude. This study highlights that consequent mass movement events are more conditioned by topographic and geo-environmental aspects such as geological structure, lithology, weathering conditions, and slope morphology, rather than exceeding specific rainfall thresholds.

Acknowledgements

This work was financially supported by the Slovenian Research and Innovation Agency (ARIS) within the research program P1-0419 ('Dynamic Earth' at the Geological Survey of Slovenia), within the research program P1-0195 ('Geoenvironment and Geomaterials' at the University of Ljubljana, Department of Geology), and within the frame of the research project "A holistic approach to the Earth surface processes driven by extreme weather events—ExtremEarth" (J7-60124). The authors acknowledge the Public Institution of Triglav National Park for allowing sampling and conducting research within the park. We also thank the Surveying and Mapping Authority of the Republic of Slovenia (GURS) for providing the aerophotographs. We thank two anonymous reviewers for their very constructive comments.

Author contributions

Conceptualization: AN, MV, AŠ; methodology: AN, MV, AŠ; fieldwork: AN, MV; visualisation: AN, MV; granulometric analysis and data interpretation: AN, AŠ; photogrammetry and data interpretation: AN, MV; writing—original draft: AN, MV, AŠ.

Data Availability

Data is available on demand.

Declarations

Competing interests The authors declare no competing interests.

References

ARSO (2006) Podnebne razmere v Sloveniji (obdobje 1971–2000). Podnebne Razmere v Slovenij (Obdobje 1971–2000). http://meteo.arso.gov.si/uploads/probase/www/climate/text/sl/publications/podnebne_razmere_v_sloveniji_71_00.pdf . Accessed 15 Mar 2022

ARSO (2021a) Climate diagram - Rateče. http://meteo.arso.gov.si/met/en/climate/diagrams/ratece/ . Accessed 22 Dec 2021

ARSO (2021b) Climate maps. http://meteo.arso.gov.si/met/en/climate/maps/ . Accessed 22 Dec 2021

ARSO (2023) Arhiv meritev. http://www.meteo.si/met/sl/archive/ . Accessed 22 Nov 2023

ARSO (2025) Povratne dobe za ekstremne padavine. http://meteo.arso.gov.si/uploads/probase/www/climate/table/sl/by_variable/return-periods/Ratece.pdf . Accessed 22 Jan 2025

Bohinec V (1935) K morfologiji in glaciologiji rateške pokrajine. Geogr Vestn 11:100–132

Celarc B (2004) Problematika »cordevolskih« apnencev in dolomitov v slovenskih Južnih Alpah Problems of the "Cordevolian" Limestone and Dolomite in the Slovenian part of the Southern Alps. Geologija 47(2):139–149. https://doi.org/10.5474/geologija.2004.011

Church M, Jakob M (2020) What is a debris flood? Water Resour Res 56(8):e2020WR027144. https://doi.org/10.1029/2020WR027144

Cruden DM, Varnes DJ (1996) Landslide types and processes. In Special Report National Research Council Transportation Research Board 247:36–75

Deline P, Alberto W, Broccolato M, Hungr O, Noetzli J, Ravanel L, Tamburini A (2011) The december 2008 Crammont rock avalanche, Mont Blanc massif area, Italy. Nat Hazard 11(12):3307–3318. https://doi.org/10.5194/NHESS-11-3307-2011

Gale L, Celarc B, Caggiati M, Kolar-Jurkovšek T, Jurkovšek B, Gianolla P (2015) Paleogeographic significance of upper Triassic basinal succession of the Tamar Valley, northern Julian Alps (Slovenia). Geol Carpath 66(4):269–283. https://doi.org/10.1515/geoca-2015-0025

Gariano SL, Guzzetti F (2022) Mass-movements and climate change. Treatise Geomorphol 546–558. https://doi.org/10.1016/B978-0-12-818234-5.00043-2

Guzzetti F, Peruccacci S, Rossi M, Stark CP (2007) Rainfall thresholds for the initiation of landslides in central and southern Europe. Meteorol Atmos Phys 98(3–4):239–267. https://doi.org/10.1007/s00703-007-0262-7

Guzzetti F, Peruccacci S, Rossi M, Stark CP (2008) The rainfall intensity-duration control of shallow landslides and debris flows: an update. Landslides 5(1):3–17. https://doi.org/10.1007/S10346-007-0112-1

Haque U, Blum P, da Silva PF, Andersen P, Pilz J, Chalov SR, Malet JP, Auflič MJ, Andres N, Poyiadji E, Lamas PC, Zhang W, Peshevski I, Pétursson HG, Kurt T, Dobrev N, García-Davalillo JC, Halkia M, Ferri S, … Keellings D (2016) Fatal landslides in Europe. Landslides 13(6):1545–1554. https://doi.org/10.1007/S10346-016-0689-3/FIGURES/10

Hooke RL (1993) The Trollheim alluvial fan and facies model revisited: discussion. Geologi- Cal Soc Am Bull 105:563–564. https://doi.org/10.1130/0016-7606(1993)105%3c0563:TTAFAF%3e2.3.CO;2

Hungr O (2005) Classification and terminology. In: Jakob M, Hungr O (eds) Debris Flow Hazards and Related Phenomena. Springer, pp 9–24

Hungr O, Evans SG, Bovis MJ, Hutchinson JN (2001) A review of the classification of landslides of the flow type. Environ Eng Geosci 7(3):221–238

Hungr O, Leroueil S, Picarelli L (2014) The Varnes classification of landslide types, an update. Landslides 11(2):167–194. https://doi.org/10.1007/s10346-013-0436-y

Jakob M, Davidson S, Bullard G, Busslinger M, Collier-Pandya B, Grover P, Lau C (2022) Debris-flood hazard assessments in steep streams. Water Resour Res. https://doi.org/10.1029/2021WR030907

Jakob M, Hungr O (2005) Debris-flow hazards and related phenomena (1st ed.). Springer Berlin Heidelberg. https://doi.org/10.1139/t05-075

Jemec Auflič M, Bezak N, Šegina E, Frantar P, Gariano SL, Medved A, Peternel T (2023) Climate change increases the number of landslides at the juncture of the Alpine. Pannonian Mediterranean Regions Sci Rep 13(1):1–14. 10.1038/S41598-023-50314-X;SUBJMETA=2739,411 1,704,844;KWRD=CLIMATE-CHANGE+IMPACTS,NATURAL+HAZARDS

Komac, B., & Zorn, M. (2007). *Pobočni procesi in človek* (D. Perko & D. Kladnik, Eds.). Geografski inštitut Antona Melika ZRC SAZU.

Maraun D, Knevels R, Mishra AN, Truhetz H, Bevacqua E, Proske H, Zappa G, Brenning A, Petschko H, Schaffer A, Leopold P, Puxley BL (2022) A severe landslide event in the Alpine foreland under possible future climate and land-use changes. Commun Earth Environ 3(1):87. https://doi.org/10.1038/s43247-022-00408-7

Margottini C, Canuti P, Sassa K (2013) Landslide science and practice. In C. Margottini, P. Canuti, & K. Sassa (Eds.), *Landslide Science and Practice*. Springer Berlin Heidelberg. https://doi.org/10.1007/978-3-642-31427-8

Novak A, Popit T, Šmuc A (2018) Sedimentological and geomorphological characteristics of Quaternary deposits in the Planica-Tamar Valley in the Julian Alps (NW Slovenia). J Maps 14(2):382–391. https://doi.org/10.1080/17445647.2018.1480975

Ogorelec B, Jurkovšek B, Šribar L, Jelen B, Božo S, Mišič M (1984) Karnijske plasti v Tamarju in pri Logu pod Mangartom. Geologija 27:107–158

Peternel T, Janža M, Šegina E, Bezak N, Maček M (2022) Recognition of landslide triggering mechanisms and dynamics using GNSS, UAV photogrammetry and in situ monitoring data. Remote Sens 14(14):3277. https://doi.org/10.3390/RS14143277

Peternel T, Urbančič T, Kozmus Trajkovski K, Grigillo D (2025) Landslide volume and runoff monitoring using UAV photogrammetry. In *Earth Observation Applications to Landslide Mapping, Monitoring and Modeling: Cutting-edge Approaches with Artificial Intelligence, Aerial and Satellite Imagery* (pp. 173–198). Elsevier. https://doi.org/10.1016/B978-0-12-823868-4.00009-X

QGIS (2021a) *QGIS*. https://www.qgis.org/en/site/ . Accessed 22 May 2021

QGIS (2021b) QGIS Python Plugins Repository. https://plugins.qgis.org/plugins/profiletool/ . Accessed 22 May 2021

Rimal R, Dhital MR, Rijal ML, Silwal R, Yadav V, Azad MA, Kainthola A (2025) Association of landslides with geological structures and rainfall: a case study of two landslides in Sunkuda, Nepal. Nat Hazards 1–20. https://doi.org/10.1007/S11069-025-07242-Y/FIGURES/13

Rossi G, Tanteri L, Tofani V, Vannocci P, Moretti S, Casagli N (2018) Multitemporal UAV surveys for landslide mapping and characterization. Landslides 15(5):1045–1052. https://doi.org/10.1007/S10346-018-0978-0/FIGURES/5

Sestras P, Badea G, Badea AC, Salagean T, Oniga VE, Roșca S, Bilașco Ș, Bruma S, Spalević V, Kader S, Billi P, Nedevschi S (2025) A novel method for landslide deformation monitoring by fusing UAV photogrammetry and LiDAR data based on each sensor's mapping advantage in regards to terrain feature. Eng Geol 346:107890. https://doi.org/10.1016/J.ENGGEO.2024.107890

Šmuc A, Janecka K, Lempa M, Kaczka RJ (2015) The spatio-temporal dynamics of the Ciprnik complex landslide, Tamar valley, Julian Alps. Slovenia. Stud Geomorphol Carpatho-Balcan 49(1):35–54. https://doi.org/10.1515/sgcb-2015-0008

Sun J, Yuan G, Song L, Zhang H (2024) Unmanned aerial vehicles (UAVs) in landslide investigation and monitoring: a review. Drones 8(1):30. https://doi.org/10.3390/DRONES8010030

Tsunetaka H (2025) Geomorphic monitoring and assessment of debris flows using drone-based structure from motion. Earth Observation Applications to Landslide Mapping, Monitoring and Modeling: Cutting-Edge Approaches with Artificial Intelligence, Aerial and Satellite Imagery 215–239. https://doi.org/10.1016/B978-0-12-823868-4.00011-8

Varnes DJ (1978) Slope movement types and processes. In R. L. Schuster & R. J. Krizek (Eds.), *Landslides, analysis and control, special report 176;Transportation Research Board Special Report* (Vol. 176, Issue 176, pp. 11–33). National Academy of Sciences.

Westoby MJ, Brasington J, Glasser NF, Hambrey MJ, Reynolds JM (2012) 'Structure-from-motion' photogrammetry: a low-cost, effective tool for geoscience applications. Geomorphology 179:300–314. https://doi.org/10.1016/J.GEOMORPH.2012.08.021

Wheaton JM, Brasington J, Darby SE, Sear DA (2010) Accounting for uncertainty in DEMs from repeat topographic surveys: improved sediment budgets. Earth Surf Process Landforms 35(2):136–156. https://doi.org/10.1002/ESP.1886

Wilford DJ, Sakals ME, Innes JL, Sidle RC, Bergerud WA (2004) Recognition of debris flow, debris flood and flood hazard through watershed morphometrics. In *Landslides* (Vol. 1, Issue 1, pp. 61–66). https://doi.org/10.1007/s10346-003-0002-0

Zorn M, Komac B (2008) Zemeljski plazovi v Sloveniji. *Georitem 8*. Založba ZRC

Supplementary Information The online version contains supplementary material available at https://doi.org/10.1007/s10346-025-02598-5.

Andrej Novak (✉)
Geological Survey of Slovenia, Dimičeva Ulica 14, 1000 Ljubljana, Slovenia
Email: andrej.novak@geo-zs.si

Marko Vrabec · Andrej Šmuc
Department of Geology, Faculty of Natural Sciences and Engineering, University of Ljubljana, Ljubljana, Slovenia